An imidazolium ionic liquid as effective structure-directing agent for the fabrication of silica thin films with vertically aligned nanochannels

Microporous and Mesoporous Materials xxx (xxxx) xxx

Contents lists available at ScienceDirect

Microporous and Mesoporous Materials

journal homepage: http://www.elsevier.com/locate/micromeso

An imidazolium ionic liquid as effective structure-directing agent for the fabrication of silica thin films with vertically aligned nanochannels

Szilvia Vavra [a], Neus Vilà [b], Antiope Lotsari [a], Alain Walcarius [b,**], Anna Martinelli [a,*]

[a] Department of Chemistry and Chemical Engineering, Chalmers University of Technology, Kemigården 4, SE-412 96, Gothenburg, Sweden
[b] Laboratorie de Chimie Physique et Microbiologie pour les Matériaux et l'Environnement, LCPME, UMR 7564, CNRS-Universite de Lorraine, 54600, Villers-les-Nancy, France

ARTICLE INFO

Keywords:
Surface active ionic liquids (SAILs)
Oriented nanochannels
Porous silica thin films

ABSTRACT

In parallel to the increasing variety of ionic liquids that show different kinds of nanometer-scale structuration in their pure and solved forms, there is a raising interest in exploring the possibility of using ionic liquids as soft-templates for the synthesis of mesoporous materials. We report the case of 1-hexadecyl-3-methylimidazolium chloride (C_{16}MIMCl), a surface active ionic liquid (SAIL), here used as an excellent soft-template for the formation of vertically aligned, uniform mesochannels, with a well defined pore width of 2.5 nm in silica thin films deposited with the electrochemically assisted self-assembly (EASA) method. The obtained mesochannels run through the entire thickness of the films and after removal of the ionic liquid the emptied mesochannels ensure a thorough mass transport to the substrate, here monitored by the redox-active electrochemical probe Ru(II)/Ru(III) during cyclic voltammetry (CV). Moreover, the mechanism of pore formation is explained; unlike the mechanisms reported for short chain imidazolium ionic liquid silica templates, in the case of C_{16}MIMCl the dominating so-called cooperative interaction is the electrostatic attraction between the $C_{16}MIM^+$ and the network-forming negatively charged silicate oligomers. Therefore, this study provides a better understanding of the templating behavior of long chain imidazolium ionic liquids and motivates further research on the synthesis of ionic liquid-based functional hybrid materials.

1. Introduction

Vertical alignment of mesochannels in silica films is highly desired in applications that utilize some sort of transport phenomena in the channel-like pores, since such a structure provides shortened, oriented diffusion pathways. Relevant applications are in separation, catalysis, electrochemical sensing, as well as optical and electrochemical devices [1,2]. Even though mesoporous silica films with vertically aligned mesochannels are challenging to realize (often channels orient parallel to the substrate), they have been successfully obtained using electrochemically assisted self-assembly (EASA) [3], evaporation induced self-assembly (EISA) [4], Stöber-solution growth [5], and epitaxial-like growth [6]. In all of these examples, a conventional surfactant was used as soft-template to result in a highly porous structure and a narrow pore size distribution.

As an alternative to conventional surfactants, ionic liquids are attracting a raising interest since they can show self-organization in dissolved or in pure form, and can hence potentially be used as soft-templates in the synthesis of mesoporous materials [7]. This is highly motivated by the idea of synthesizing functional hybrid materials in which the organic ionic liquid provides an added function besides templating the inorganic matrix. Also, for some applications (e.g. in electrochemical devices) the immobilization of the ionic liquid within the inorganic matrix is favourable simply to prevent leakage and provide appropriate mechanical properties [8].

The soft-templating function of certain ionic liquids originates from their unique molecular structure. In general, ionic liquids consist of ionic species with significant molecular asymmetry in at least one of the ions, which disfavors ordering of the ions into solid crystalline phases resulting in low melting temperatures (by definition under 100 °C) [9–11]. Nevertheless, nano-structuration can occur in pure ionic liquids, in their mixtures with other molecular solvents, or in solvated form at different extent regarding the length scale, shape and kinetics, with very wide variety among ionic liquids determined by their specific molecular

* Corresponding author.
** Corresponding author.
E-mail addresses: alain.walcarius@univ-lorraine.fr (A. Walcarius), anna.martinelli@chalmers.se (A. Martinelli).

https://doi.org/10.1016/j.micromeso.2020.110407
Received 17 March 2020; Received in revised form 25 May 2020; Accepted 15 June 2020
Available online 8 July 2020

structure [7,12]. Despite these properties, using ionic liquids as templates in the synthesis of mesoporous silica is not straightforward, and experiments have shown that the intrinsic structuration of ionic liquids is not always sufficient for the formation of mesopores in the silica network. Moreover, a cooperative interaction between the template and the precursor is often crucial in achieving a desired mesoporosity [13,14]. For example, the sol-gel synthesis of silica using a short-chain imidazolium ionic liquid as the co-solvent usually leads to the formation of ionogels based on non-porous silica particles, despite the present supramolecular (e.g. ion cluster) and mesoscopic range (e.g. micro-phase separation, H-bond network) structurations in the ionic liquid [8,12,15]. An exception among short-chain imidazolium ionic liquids is $[C_4MIM]^+[BF_4]^-$, which has successfully been used as soft-template in the sol-gel synthesis of mesoporous silica under water-poor, acidic condition by Zhou et al. [14]. The templating effect was explained with the so-called hydrogen bond-co-π-π stack mechanism, which involves hydrogen bonds formed between the $[BF_4]^-$ anions and the silanol groups of silica and the π-π stack interactions of the neighboring imidazolium rings of the cations. The obtained mesoporous monolith contained worm-like pores in which the $[BF_4]^-$ anions are assumed to be located along the pore walls while the imidazolium rings of the cations arrange next to the anions due to electrostatic attraction and are stacked parallel to each other due to π-π interactions, and the hydrophobic alkyl chains point towards the centre of the pores.

Compared to the case of short-chain imidazolium ionic liquids, there are a few more, yet limited in number, examples of syntheses where long-chain imidazolium ionic liquids have been used as soft-templates to obtain mesoporous silica. In long-chain imidazolium ionic liquids, the longer alkyl chain enhances the amphiphilic nature of the cation and the behavior of the ionic liquid approaches that of surfactants. These ionic liquids are also referred to as surface active ionic liquids (SAILs) [16]. Within the subgroup of alkyl-imidazolium ionic liquids with the chloride anion, $[C_6MIM]^+[Cl]^-$ is considered the "transitional ionic liquid", since it shows surface activity but no self-assembly in water [16]. More amphiphilic ionic liquids, that show an amphiphilic self-assembly in an aqueous medium, are more suitable soft-templates for the formation of different mesoporous silica structures *via* the sol-gel process (using water as the solvent) [17]. With the $[C_nMIM]^+[Br]^-$ ionic liquid group, where n is the number of carbon atoms in the straight alkyl chain attached to the imidazolium head, wormlike (n = 8–12) and hexagonal (n = 14–16) mesoporous silica could be prepared [18]. With $[C_{16}MIM]^+[Cl]^-$, MCM-type hexagonal (MCM-41, with p6mm symmetry) and cubic gyroid (MCM-48, with Ia3d symmetry) silica could be obtained by tuning the ionic liquid concentration in the aqueous reaction solution [17]. Besides, $[C_nMIM]^+[Cl]^-$ ionic liquids were able to form a lamellar pore structure in monolithic mesoporous silica, with the pore diameter being determined by the alkyl chain length and ranging from 1.2 nm (n = 14) to 1.5 nm (n = 18) [19,20].

Even though more and more empirical information is gained on silica-templating with long-chain imidazolium ionic liquids during the sol-gel process, the underlying mechanism is often not studied nor even discussed. Fortunately, $[C_{16}MIM]^+[Cl]^-$ has many similarities with CTAB (cetyltrimethylammonium bromide), which comes handy in experimental design and basic understanding. However, there are also differences that can become relevant when a specific pore structure or reaction condition is required [13]. It has been already described that during the sol-gel mesoporous silica synthesis in an aqueous reaction solution the cooperative interaction between the template and the precursor is crucial for pore formation on the nanometer scale [13,17]. In general, when the template is CTAB, at basic pH this cooperative interaction is dominantly the electrostatic attraction between the cation of the surfactant ($[CTA]^+$) and the framework-forming negatively charged silicate oligomers [17]. It may be proposed that the same electrostatic attraction occurs between $[C_{16}MIM]^+$ and the silicate oligomers under similar reaction conditions [17]. This is however not an obvious hypothesis since, in contrast to the ammonium head, the imidazolium head is capable of establishing further interactions; as schematically illustrated in Fig. 1 [15]. It is known that the imidazolium cation is able to establish hydrogen bonds with negative charge centers, primarily through the C^2H site [21–23], while the presence of hydrogen bonds between the imidazolium head group and the silica precursor has been proposed by Kaper et al. in agreement with a study by Wang et al. [13,17]. Another characteristic of the imidazolium cation is the ability to arrange parallel, in a layering structure, due to π-π interactions, which dominates on the short length scale (~10 Å) with little influence of proximate interfaces [24,25]. This results in a higher packing density and a higher tendency to form mesostructures with a lower curvature [13,17]. Interestingly, CTAB and $[C_{16}MIM]^+[Cl]^-$ in fact show very similar critical micellar concentrations (c.m.c.) and enthalpies of micellization (note that the binding affinity of the bromide ion is slightly higher than that of the chloride ion) [13].

The main aim of this study is to demonstrate that it is possible to achieve vertically aligned mesochannels inside thin films of silica by using $[C_{16}MIM]^+[Cl]^-$ as soft template during the EASA process (Fig. 2). Already established methods are used to verify the obtained structures. Briefly, during EASA fast condensation of the pre-hydrolysed silica precursor in the presence of a templating agent occurs on a cathodic electrode, where the locally generated hydroxyl ions catalyze the condensation reaction [3]. The formation of the silica network is much more rapid than in the other methods mentioned above, which is relevant for retaining the nano-structure of the ionic liquid that in turn has an impact on the pore formation [1,3]. To the best of our knowledge, no other surfactant than CTAB and no ionic liquid have ever been successfully used in EASA, hence this work is a significant contribution to an area that has remained unexplored, and provides new insights. By showing that the EASA method can be extended to the use of ionic liquids as templates, we can better understand the reaction mechanisms but also propose an avenue to realize new ionic liquid-based functional hybrid materials. As for the latter, we take a special interest in developing materials with desired transport properties, targeting fast proton motion in nanoscaled pores. For this purpose, however, purely protic ionic liquids or a mixture of $[C_{16}MIM]^+[Cl]^-$ and a protic ionic liquid should be used, which will be the scope of future studies.

2. Experimental section

2.1. Chemicals

For the synthesis of thin films of mesoporous silica the following reagents were used: tetraethoxysilane (TEOS, 98%, Alfa Aesar) as the precursor, ethanol (95–98%, Merck) as the co-solvent, $NaNO_3$ (>99%, Prolabo) as the electrolyte salt, HCl (1 M in aqueous solution, VWR) for pH adjustment and the ionic liquid 1-hexadecyl-3-methylimidazolium chloride ($C_{16}MIMCl$, >98%, Iolitec - Ionic Liquid Technologies GmbH) as the templating agent. Ruthenium hexamine chloride ($[Ru(NH_3)_6^{3+}][Cl^-]_3$, 98%, Sigma Aldrich) was used as a redox-active electrochemical

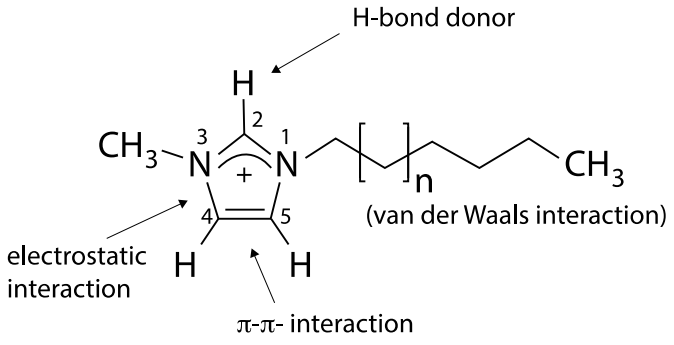

Fig. 1. Schematic of the possible interactions that the 1-alkyl-3-methyl-imidazolium cation is able to establish. Reproduced from Ref. [15].

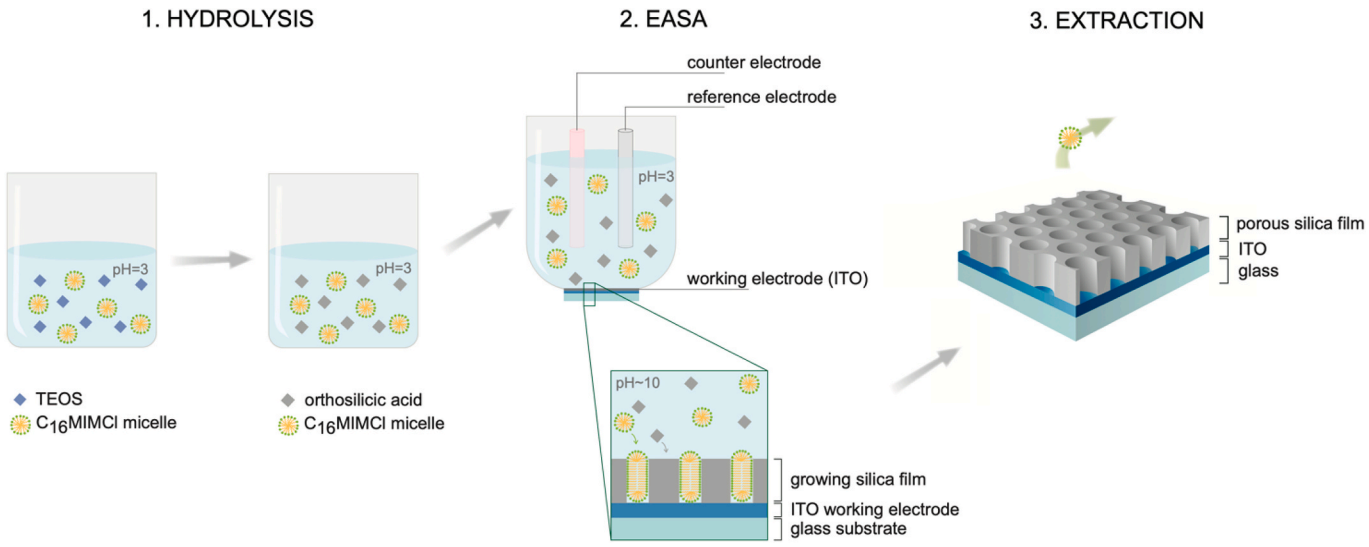

Fig. 2. Schematic illustration of the subsequent steps involved in the synthesis of IL-templated mesoporous silica thin films using the EASA method.

probe. All solutions were prepared with high purity water (18 MΩcm^{-1}) from Purelab Option-Q water purification system (ELGA).

2.2. Preparation of mesoporous thin films

The ionic liquid (IL)-templated mesoporous silica thin films were synthetized *via* the electrochemically-assisted self-assembly (EASA) method (Fig. 2). First, a solution was prepared with 100 mM TEOS, 0.1 M $NaNO_3$ in 40 ml ethanol:water (1:1) mixture with C_{16}MIMCl added at various IL/TEOS ratios (reported in mol/mol), i.e. 0.32, 0.64, 1.28, and 1.60. The solution was adjusted to pH 3 with 0.1 M HCl and stirred for 2.5 h at room temperature for the prehydrolysis of TEOS. The potentiostatic deposition on an indium tin oxide electrode (ITO, surface resistivity 8–12 Ω, Delta Technologies) was carried out in a three-electrode system consisting of ITO as the cathodic working electrode, silver wire as the pseudo-reference electrode and stainless steel as the counter electrode. The potential was applied using a μAutolab III potentiostat (Eco Chemie). The deposition of a silica film on ITO could be observed at an applied voltage of −1.55 V, while the deposition time was 20 s. The delivered current was recorded as a function of time during deposition, and was found to be slightly higher than previously reported for EASA syntheses with CTAB (see Fig. S1 in the SI) [3]. After deposition, the films were rinsed with water and aged at 130 °C in a vacuum oven, overnight. Rinsing with water has the effect of removing siliceous species possibly left on top of the deposited films, which may otherwise attach to the surface by further condensation. After aging, extraction of the IL was carried out on some of the samples for every IL/TEOS ratio by immersing the deposited film into a solution of 0.1 M HCl in ethanol for 20 min, followed by rinsing with pure ethanol. The names given to the samples and the details of preparation are listed in Table 1.

Table 1
Sample names, reflecting the IL/TEOS ratio used in the deposition solution and the treatment applied after ageing.

Sample Name	IL/TEOS ratio (mol/mol)	Treatment after aging
0.32 NE	0.32	none (not extracted)
0.32 E	0.32	extracted
0.64 NE	0.64	none (not extracted)
0.64 E	0.64	extracted
1.28 NE	1.28	none (not extracted)
1.28 E	1.28	extracted
1.60 NE	1.60	none (not extracted)
1.60 E	1.60	extracted

2.3. Morphological characterization

Scanning electron microscopy (SEM) images were obtained with a JEOL 7800F Prime microscope (using a 5 kV acceleration voltage) on extracted samples. Before imaging, the samples were coated with palladium using an EMITECH K550x sputter coater. Cross sectional samples were prepared by breaking the substrate after sputtering and imaging the broken surface on a tilted SEM stage.

For top view TEM (transmission electron microscope), the samples were prepared by placing a droplet of sludge from extracted, grinded films on a carbon-coated Cu TEM grid and dried overnight under ambient conditions. The TEM experiments were performed on a FEI Tecnai T20 instrument operating at 200 kV, and the obtained images were processed with the Digital Micrograph software to determine pore widths. For the cross-sectional TEM study, a sample of a thin film (namely 0.32 E) was prepared with the liftout technique using a focused ion-beam coupled SEM (FEI Versa Dual FIB/SEM).

Grazing incidence small angle X-ray scattering (GISAXS) measurements were performed on a Mat:Nordic instrument from SAXSLAB/Xenocs. The X-ray beam was produced by a Cu-radiation source and focused with a Micro-Max 003 X-ray generator from Rigaku. Pilatus 300K from Dectris was used as the detector. The samples were placed on a GISAXS holder and aligned before each measurement. The sample to detector distance was 305 mm, the incidence angle 0.2°, and the exposure time 20 h. Scattering patterns were collected before and after measurement for 20 min to make sure that no radiation damage occurred. The collected 2D scattering patterns were further processed with the SAXSGUI (Rigaku) software by horizontal integration of intensities performed between $q_z = 0.01$ Å^{-1} and $q_z = 0.06$ Å^{-1}, and subsequent plotting as a function of q_y. Multi-peak fitting using the Igor software was used to determine exact peak positions. The cell parameters of the hexagonally ordered porous structures were determined based on references [26,27] and are given in Table S1 and Table S2 of the SI file.

2.4. Chemical characterization

X-ray photoelectron spectroscopy (XPS) was carried out on Quantum 2000 scanning ESCA microprobe from Physical Electronics with AlKα (1.486 keV) beam at an incidence angle of 45° relative to the sample surface. The MultiPAK software package was used to determine the atomic concentration. Photoelectrons were collected on approximately 500 × 500 μm^2 large areas.

Vibrational spectra were recorded with a PerkinElmer Fourier transform infrared (FT-IR) spectrophotometer in the reflection-absorption mode, sometimes also referred to as IRRAS (InfraRed Reflection Absorption Spectroscopy), which is the most suitable to study thin films on metal surfaces. Because the films investigated here are thin (below 100 nm) and the ITO substrate acts in the infrared as a metallike mirror, the obtained spectrum resembles (unlike other reflectance modes) the one that would be obtained in pure transmission mode from the free standing film. The measured spectral range was 4000 cm^{-1}–400 cm^{-1} and the resolution was set to 4 cm^{-1}. For all experiments, 64 scans were collected and averaged, while the ITO substrate without any film deposited was used as a reference for the background subtraction. For presentation purposes, the recorded data were baseline corrected.

2.5. Permeability of the films

The permeability of the deposited films to cations, here Ru(III), was studied by cyclic voltammetry. The measurements were carried out in a three-electrode system that contained a stainless steel counter electrode, a Ag/AgCl reference electrode (Metrohm), and a bare ITO plate or ITO plate with the deposited silica film on it as the working electrode. The aqueous electrolyte solution contained 0.5 mM $Ru(NH_3)_6^{3+}$ and 0.1 M $NaNO_3$, while the contact area with the solution was 0.5 cm^2. The voltammogram curves were recorded with a μAutolab III potentiostat (Eco Chemie) at a scan rate of 20 mV/s.

3. Results and discussion

3.1. Pore formation with an imidazolium-based IL template

The electrochemically assisted self-assembly (EASA) of silica thin films in the presence of a long-chain aprotic ionic liquid, C_{16}MIMCl, resulted in vertically ordered mesoporous channels running through the entire silica film thickness. Based on morphological characterization, the formation of mesochannels was observed on all silica thin films that were deposited from solutions with an IL/TEOS ratio between 0.32 and 1.60.

The local structure of these mesochannels can be observed on the TEM image of the cross-sectional sample prepared with the lift-out technique. It reveals that individual channels in the silica film are vertical to the ITO substrate and can reach its surface in direct contact (Fig. 3A). A complementary top view TEM image also shows that these channels are not only well-separated, but also hexagonally ordered (Fig. 3B). These TEM images were processed using the Digital Micrograph software, by which the pore width was determined to be approximately 2.5 ± 0.3 nm, a dimension that is independent of the IL/TEOS ratio used in the deposition solution (see Fig. S2 in the SI). This dimension is similar to the size of two adjacent hexadecyl-tails and it can be assumed that the IL has a core-shell packing in the pores with the hydrocarbon tails forming the core and the charged heads forming the outer shell [10,28]. Furthermore, based on cross sectional SEM images, the IL-templated silica thin films are shown to be deposited as even, continuous layers, without any cavities between the film and the substrate (Fig. 3C; see also Fig. S3 in the SI). In addition, SEM and TEM images revealed that the films' thickness is around 70 nm. Also, SEM images show the presence of nanoparticles on top of the films (Fig. 3C and D; see also Fig. S3 in the SI). These are side products of the EASA process and their presence has been described in the literature also for other EASA-prepared films [29].

Grazing-incidence X-ray scattering patterns of the IL-templated silica films confirm that the presence of vertically oriented, hexagonally ordered pore morphology is the long-range, dominating pore structure in the films. In fact, the highest scattering intensities originate from the vertical mesochannels resulting in peaks along the q_y scattering vector characteristic both in shape and position (Fig. 4; see also Fig. S4 in the SI) [29,30]. Moreover, after processing the 2D scattering patterns with horizontal integration, the intensity peaks could be assigned to the (10), (11), (20) and (21) reflections of the hexagonal lattice of the pores (Fig. 4B). Indeed, the relation between the position of the scattering peaks $q_y(10):q_y(11):q_y(20):q_y(21)$ is consistent with the relation

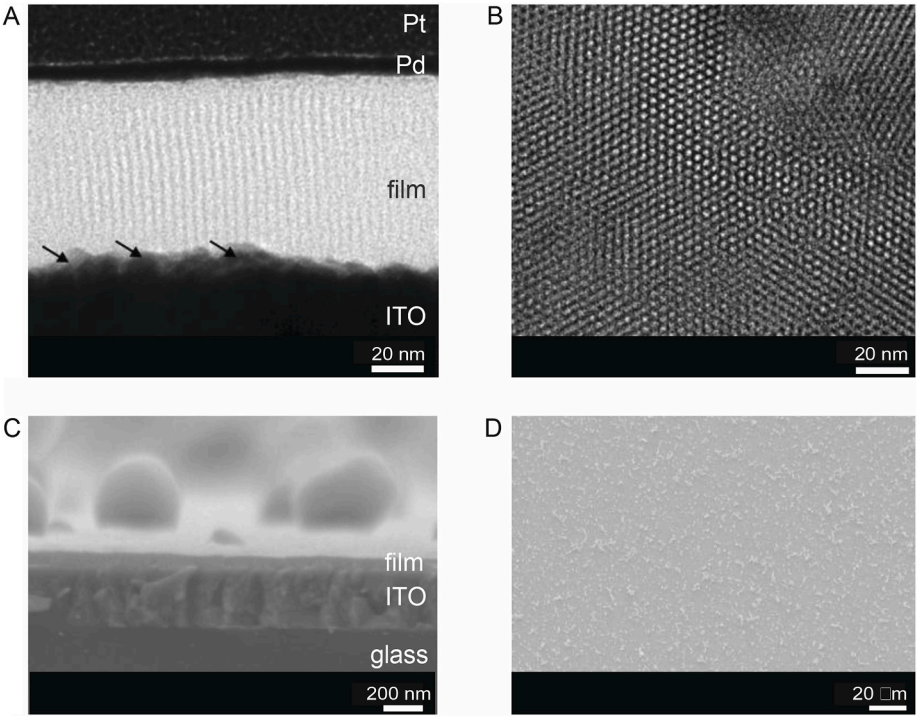

Fig. 3. Electron microscopic images of the IL-templated silica thin films after extraction. A: cross-sectional TEM image of a 0.32 E sample prepared with the lift-out technique. The arrows point to the interface between the thin film and ITO; B: top-view TEM image of a 0.32 E sample; C: cross-sectional SEM image of a 0.64 E sample on its substrate; D: top-view SEM image of a 0.64 E sample.

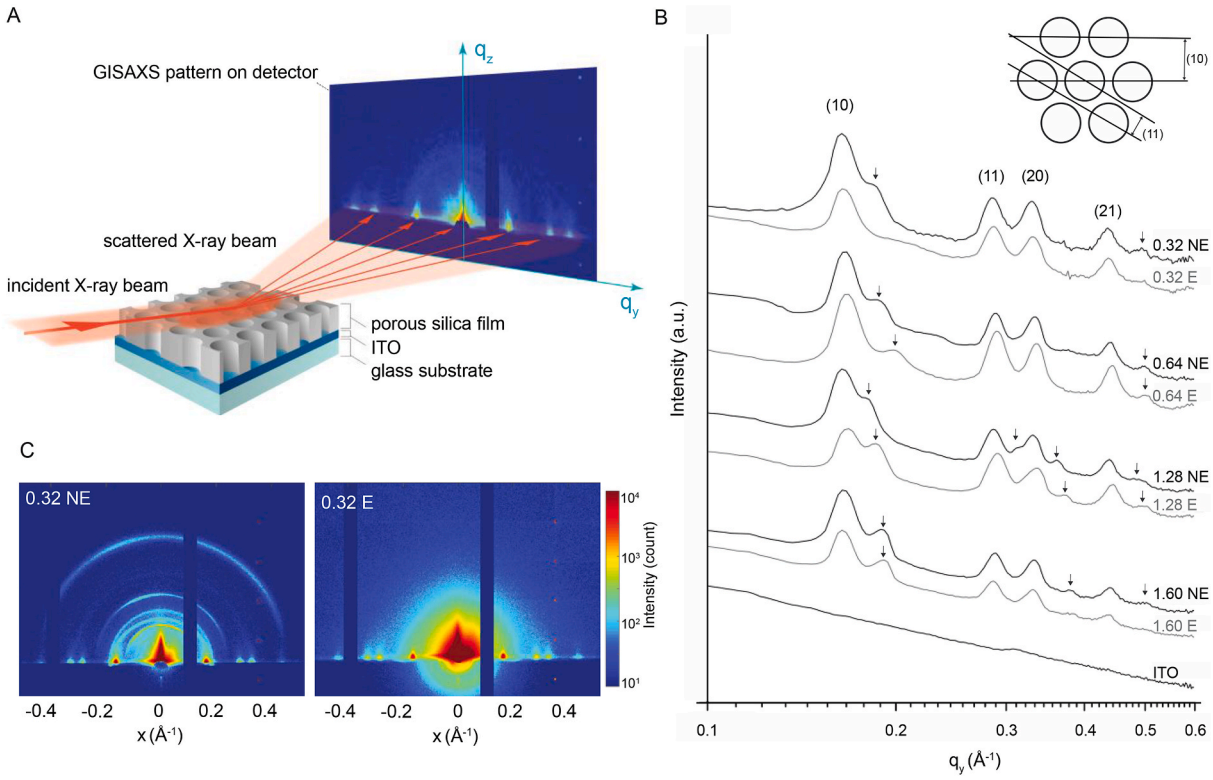

Fig. 4. Grazing-incidence X-ray scattering of the IL-templated silica thin films. A: Schematic of a GISAXS measurement of a silica thin film with vertically-aligned channel-like pores. B: Horizontally integrated X-ray scattering intensities of different silica thin films (integration performed between $q_z = 0.01$ Å^{-1} and $q_z = 0.06$ Å^{-1}). C: Selected 2D X-ray scattering patterns, i.e. for a sample before (0.32 NE, left) and after (0.32 E, right) the extraction of the IL.

$1 : \sqrt{3} : \sqrt{4} : \sqrt{7}$, which is characteristic of the hexagonal p6m symmetry, here describing the channel-to-channel spacing [31,32] (see also Table S1 in the SI). In addition, the elongated shape in the q_z direction reveals a domain size of the hexagonal phase larger than the thickness of the film (see Fig. 4C), which can be observed on the TEM images of the films as well (see Fig. 3B and also Fig. S2 in the SI) [30]. Furthermore, it is important to underline that there was no significant shift in the q_y peak positions in films characterized before and after extraction, indicating that the pore morphology remains unchanged upon extraction of the ionic liquid and demonstrating the stability of the silica network (see Table S1 in the SI). Interestingly, the position of the q_y scattering vectors are independent also on the IL/TEOS ratio of the deposition solution, showing a (10) lattice spacing of ≈3.8 nm, a (11) lattice spacing of ≈2.2 nm, and a cell parameter between 4.3 and 4.4 nm for all IL-templated silica films. This cell parameter is similar, but slightly higher, than the cell parameter of 4.1 nm found for CTAB-templated silica films prepared with EASA [29].

Next to the characteristic scattering pattern along the q_y axis, there are weak-intensity rings on the 2D X-ray scattering patterns (Fig. 4C; see also Fig. S4 in the SI). The appearance of these rings can be explained by the silica nanoparticles observed on top of the films (see also the SEM images) having mesopores with comparable size to the mesochannels in the films. As these pores are oriented randomly they scatter X-rays also in q_z direction forming a ring-shaped pattern. Also, it can be seen on the 2D scattering patterns that the intensity of the rings is lower for the extracted samples, indicating the partial removal of the particles (Fig. 4C; see also Fig. S4 in the SI). The presence of these rings is reflected by the appearance of additional lower intensity peaks, marked by short arrows in Fig. 4B. Since these additional peaks have positions in the q axis that match relatively well the above mentioned ratios typical of the hexagonal p6m symmetry, we propose that also the spherical particles possess the hexagonal phase, although randomly oriented in space (see also Table S2 in the SI). The peak positions also reveal that the hexagonal phase in the particles has lower lattice spacing and cell parameter than the hexagonal phase in the film. These particles are an undesired product of the deposition reaction and, as already discussed in Ref. [29], can be minimized by controlling the synthesis parameters such as deposition time, cathodic potential and concentration of the silane precursor. When using C_{16}MIMCl as the soft template, a shorter deposition time (e.g. of 15 s) may result beneficial and future works will reveal if this is the case.

From the detailed morphological characterization we found that the hexagonally ordered, vertically oriented, channel-like pore morphology formed by C_{16}MIMCl is similar to the pore morphology of the CTAB-templated, EASA-deposited silica films, previously reported by Walcarius et al. [3,33]. The similarity of the two amphiphiles is intriguing. It is known that the morphology of the silica films deposited with CTAB is extremely sensitive to synthesis parameters (e.g. TEOS concentration, type and amount of co-solvent, salt composition and concentration) [29], which all influence the self-assembly of CTAB both in bulk and at the surface during deposition. We observe here that for a selected set of synthesis parameters, the use of the ionic liquid C_{16}MIMCl instead of CTAB results in the same pore morphology of the film with the only difference that a higher voltage had to be applied during EASA [32,33]. This indicates that self-assembly of C_{16}MIMCl, and therefore supposedly also its packing parameter, is very similar to that of CTAB under the synthesis conditions of EASA and that C_{16}MIMCl can be used as templating agent for mesochannel formation as successfully as CTAB. A further important note is that, to the best of our knowledge, C_{16}MIMCl is the only other surfactant-like molecule, besides CTAB, with which vertically oriented mesochannels could be achieved in EASA-deposited silica thin films. Also, the reported films are the first ionic liquid templated mesoporous silica films that contained separated mesochannels oriented perpendicularly to a substrate.

3.2. Chemical composition before and after extraction

Based on elemental analysis done with XPS measurements, the chloride anion of the IL was undetectable in the silica thin films deposited from reaction solutions with IL/TEOS ratios between 0.32 and 1.28 (see Table S3 in the SI). Moreover, in the IR spectra of these samples after extraction, the ν_{O-H} (~ 3400 cm^{-1}) stretching vibration peak appears and the intensity of the ν_{Si-OH} (~ 950 cm^{-1}) stretching vibration slightly increases, the latter reflecting an increased abundance of silanol bonds (Si–OH) in the extracted films (Fig. 6A). Thus, based on XPS and IR results, it can be assumed that on the silica pore wall of as synthetized thin films the silanol groups are deprotonated, having their negative charges neutralized by the $C_{16}MIM^+$ cations, as schematically depicted in Fig. 5. From this, it can be proposed that attractive electrostatic interactions between the $C_{16}MIM^+$ cations and the silicate oligomers had crucial role in the formation of the mesoporous structure. These results also suggest that at the extraction step, aimed to remove the $C_{16}MIM^+$, the negatively charged silica wall gets protonated by the hydrochloric acid of the extraction solution resulting in the intensity rise of the ν_{Si-OH} peak. Notably, the chloride ion was detectable by XPS only in the 1.60 NE sample, but its IR, GISAXS, and electron microscopic data are equivalent to those of the other samples, which implies that the XPS results may simply be contamination from the extraction solution.

Full removal of $C_{16}MIM^+$ *via* extraction was confirmed by IR, since the alkyl chain ν_{C-H} (2960–2855 cm^{-1}) stretching vibrations and the imidazolium ring δ_{ring} (1570 cm^{-1}) bending vibrations disappear from the IR spectra of the extracted samples (Fig. 6A). From this, it follows that the $C_{16}MIM^+$ cations are located only in the mesochannels of the films and do not get entrapped in the bulk silica network.

The amorphous structure of the deposited silica films is demonstrated by several features in their IR spectra, especially in the 1300–900 cm^{-1} region (Fig. 6B). In general, sol-gel derived silica films display a characteristic longitudinal optic–transverse-optical (LO-TO) splitting of the $\rho_{Si-O-Si}$ (507–457 cm^{-1}), the $\nu_{s(Si-O-Si)}$ (820–810 cm^{-1}), and the $\nu_{as(Si-O-Si)}$ (1250–1070 cm^{-1}) vibrational modes [34]. In the IR spectra recorded from the IL-templated silica thin films studied here, the $\nu_{as(Si-O-Si)}$ LO-TO splitting results in two strong peaks at 1230 cm^{-1} and ~1105 cm^{-1}. It is worth to mention that the LO peak usually appears as a high frequency shoulder of the TO mode, and is enhanced when the IR light has lower incident angles with respect to the film's surface. Its significant intensity (relative to the TO mode) in the IR spectra shown in Fig. 6 can also be explained by the occurrence of scattering within the pores [34], which is congruent with the porous structure of the synthesized thin films already shown by TEM and GISAXS results. Also, both the $\nu_{as(Si-O-Si)}$ (LO) and the $\nu_{as(Si-O-Si)}$ (TO) modes show considerable widths indicative of a wide distribution of Si–O–Si bond angles and bond lengths. After extraction, the shift of the $\nu_{as(Si-O-Si)}$ (TO) mode to higher frequencies indicates the increase in Si–O–Si bond angles in the silica network. A further feature that we observe in the amorphous silica, is the rise of a feature at ~1200 cm^{-1} between the $\nu_{as(Si-O-Si)}$ LO and TO peaks, also referred to as the "disorder-induced" mode [34]. In addition, the LO and TO modes increase in intensity after extraction, which could be due to further condensation catalyzed by the acidic medium (used for the extraction) and/or enhanced scattering in the emptied pores. We can also conclude that dangling silanol groups are located not only on the pore walls, but also in the bulk silica phase since the ν_{Si-OH} (~ 950 cm^{-1}) stretching mode appears in both extracted and non extracted samples. Furthermore, the shoulder of $\nu_{as(Si-O-Si)}$ (TO) at 1050–1100 cm^{-1} can be related to the presence of nonbridging oxygens in the network. A final note is that water was not detected by IR in the IL-templated silica thin films before extraction (NE samples), suggesting that the included ionic liquid imparts hydrophobicity to the synthesized material. By contrast, the IR spectra after extraction (E samples) show the typical bending mode of water at 1635 cm^{-1} as well as an intense and broad feature peaked at ~3400 cm^{-1} due to H–O–H stretching modes. To a minor degree, O–H stretching modes of the SiO–H groups also contribute to this latter feature.

3.3. Permeability of the films

The quality of the deposited films in terms of ion permeation through the mesochannels before and after removal of the ionic liquid was investigated by monitoring the transport properties of a redox-active electrochemical probe, here the Ru(III) cation, with cyclic voltammetry (Fig. 7). On the voltammogram recorded with bare ITO, the negative peak current on forward scan indicates reduction of $[Ru(NH_3)_6]^{3+}$ to $[Ru(NH_3)_6]^{2+}$ and the positive peak on scan reversal corresponds to the oxidation of $[Ru(NH_3)_6]^{2+}$ to $[Ru(NH_3)_6]^{3+}$ [35]. The measured current was close to null when recorded on silica thin films that still contained $C_{16}MIM^+$ in its mesochannels (not extracted samples) (Fig. 7A). This shows that the redox reactions of the ruthenium ions are hindered due to restricted or blocked diffusion pathways through these films towards the ITO layer. For the silica thin films that were generated from solutions with a IL/TEOS ratio of 0.64 or higher, no significant current was measured at all in the applied voltage range, thus they behave as insulator layers impeding the ruthenium ions to reach the electrode. However, when the deposition solution had a IL/TEOS ratio of 0.32, the CV curve of the silica thin film sample (0.32 NE) showed a small but measurable current with peak positions close to the reduction and oxidation peaks measured on bare ITO. The appearance of these low current peaks can be explained by an imperfect coverage of the film on the electrode (note that GISAXS and IR results are equivalent to the other non-extracted samples) resulting in ruthenium ions able to reach the electrode but only to a limited extent. Moreover, due to the presence of $C_{16}MIM^+$ in the mesochannels, the probe molecules display an impeded diffusion, which is reflected by the low current values and the increased peak-to-peak separation (ΔE_p) as compared to the bare ITO electrode (see Table S4 in the SI). Nevertheless, from the well-insulating behavior

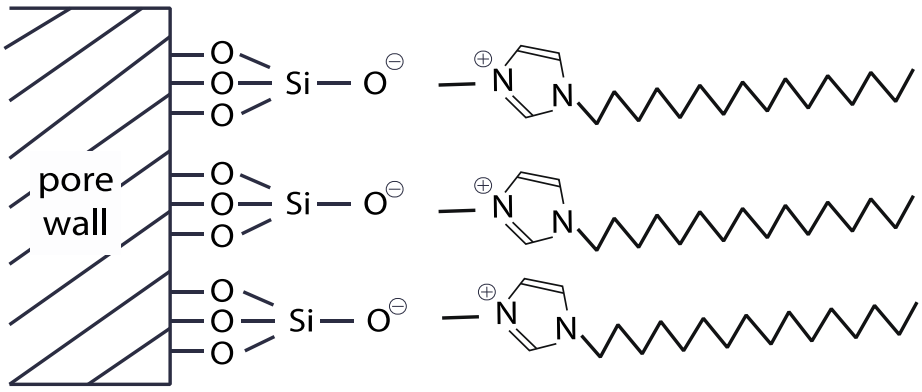

Fig. 5. Schematic of the proposed neutralization of the negatively charged silica wall by $C_{16}MIM^+$ cations in the mesochannels of the IL-templated silica thin films.

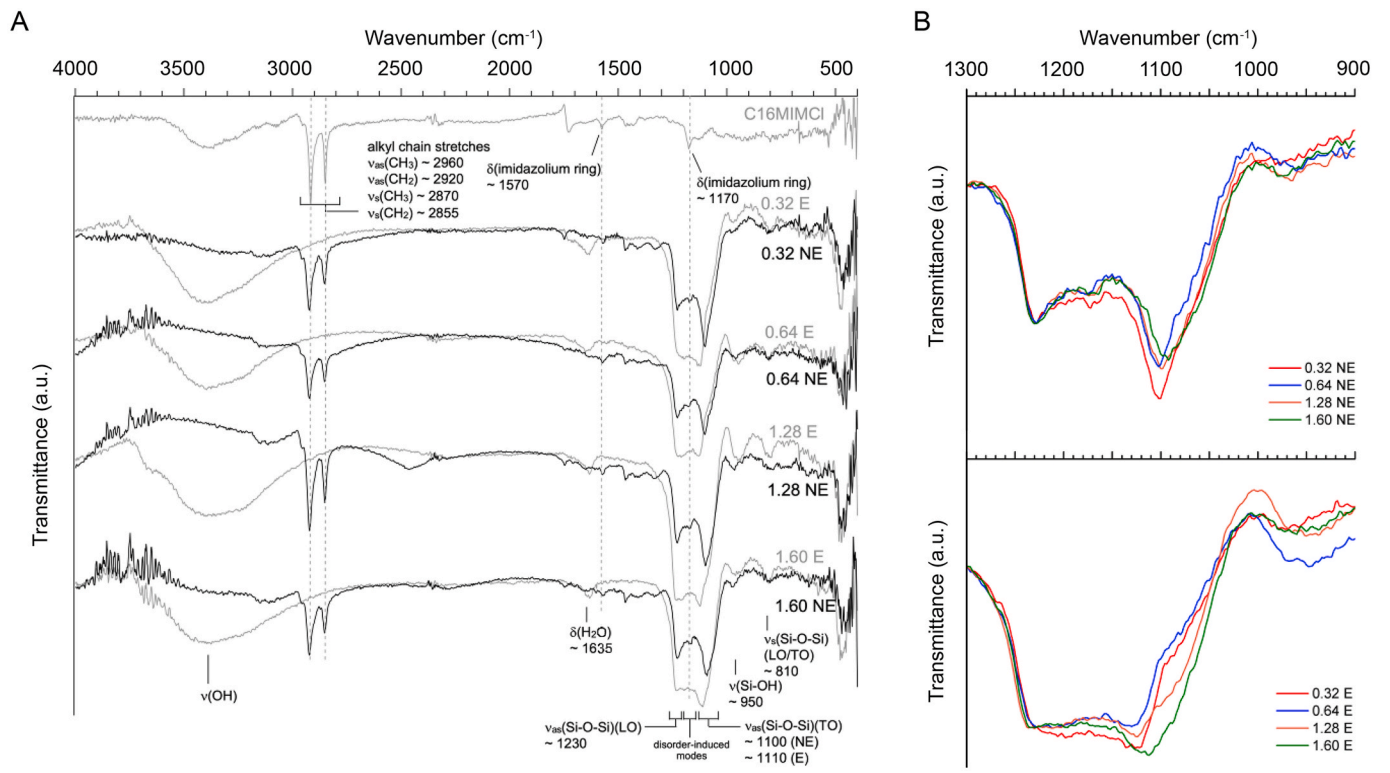

Fig. 6. A: Infrared spectra collected with an oblique incidence angle from the IL-templated silica thin films. B: Close up of the 1300-900 cm^{-1} region of the IR spectra presented in A.

of the films deposited from solution with an IL/TEOS ratio of at least 0.64, two important features of the films can be described. Firstly, these insulating films have full coverage of the surface and good contact with the ITO, the latter can be observed locally on SEM images as well. Secondly, the cation of the IL, $C_{16}MIM^+$, does not diffuse upon cathodic potential therefore no significant current occurs and $C_{16}MIM^+$ remains insoluble for the contacting aqueous solution. This shows that there is strong electrostatic attraction between the negatively charged silica wall and the $C_{16}MIM^+$ cation that prevents not only the diffusion of the $C_{16}MIM^+$ ion, but also the penetration of the Ru(III) cation through the pores.

After removal of the $C_{16}MIM^+$ from the mesochannels, the IL-templated silica thin films show drastically changed permeability properties (Fig. 7B). On the cyclic voltammograms of the extracted samples both oxidation and reduction peaks of the ruthenium redox probe appeared, quite similar to the case of bare ITO. This indicates that the ruthenium ions could reach the ITO electrode through the empty mesochannels. Moreover, the slightly larger measured currents on film electrodes can be rationalized with the shorter diffusion pathways of ruthenium ions enabled by the straight mesochannels directing towards the electrode and supposed accumulation of the ruthenium ions due to interactions with the silica wall as previously described in the literature [35].

To summarize, the CV curves shown in Fig. 7 demonstrate the existence and accessibility of aligned mesochannels in the films. The general permeability properties of these films are expected to be similar to those of previously reported equivalent structures, obtained by either the EASA or the Stöber method, which have been extensively studied [32, 36–40].

The selectivity of the mesopores is another interesting aspect that could be investigated more thoroughly by using negatively charged or neutral probe species. Albeit being outside the scope of the current work we can anticipate that, given the negative charge of the pore walls in the film structure, using anionic redox probes such as the couple $[Fe(CN)_6]^{3-}/[Fe(CN)_6]^{4-}$ should result in reduced electrochemical response compared to the case of bare ITO, due to electrostatic repulsion and hence suppressed ingress of the anions. This, including the effect of ionic strength, has been reported for CTAB-based films by Karman et al. [39] and is thus not reproduced here.

Since it is well known that silica films with vertically ordered mesochannels exhibit molecular sieving properties and permselective ion transport [40,41] redox probes can also be chosen with the specific aim to determine the diameter of the available pores and their structural stability. For instance, cationic fluorophores of similar geometries but different sizes have been used to evidence permeation through (i.e. ruthenium trisbipyridine, $Ru[bpy]_3^{2+}$, and ruthenium trisphenanthroline, $Ru[phen]_3^{2+}$, molecular size of 1.3 nm) and exclusion from (i.e. ruthenium trisdiphenylphenanthroline, $Ru[dpp]_3^{2+}$, 2.0 nm in diameter) a mesoporous silica membrane [42].

4. Conclusions

The presented study extends the possibility of templating silica to the use of ionic liquids, which is a developing field with the potential of producing ionic liquid-based functional hybrid materials. In our approach, we used a long chain imidazolium ionic liquid during the EASA method to deposit mesoporous silica thin films. Our results reveal that during the silica film deposition $C_{16}MIMCl$ forms vertically aligned, distinct mesochannels with a well defined pore size and a highly packed hexagonal arrangement. Moreover, these mesochannels run through the entire film thickness enabling mass transport through the film and a robust contact with the substrate after removal of the templating ionic liquid. Important information on the mechanism of pore formation has been gained as well; in-depth characterization of the film shows that there is electrostatic attraction between the pore forming $C_{16}MIM^+$ ions and the negatively charged silica pore wall, which reasonably originates from the electrostatic attraction between the $C_{16}MIM^+$ and the network-forming negatively charged silicate oligomers. Furthermore, it can be

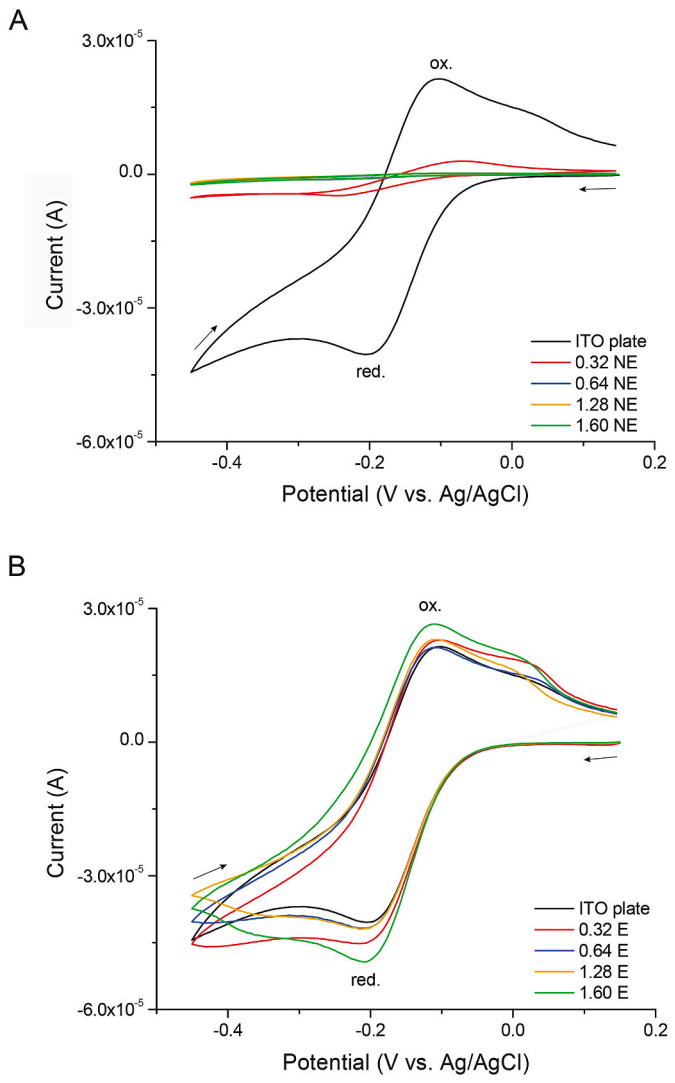

Fig. 7. Cyclic voltammetry curves recorded in a Ru(III) solution using a bare ITO electrode and ITO electrodes covered with the IL-templated silica thin films, before (A) and after (B) extraction of the IL.

proposed that the described electrostatic attraction is the main so-called cooperative interaction during pore formation as C_{16}MIMCl and CTAB form mesochannels with high curvature at the same range of template-to-precursor ratio in the deposition solution. This also indicates that π-π interactions and hydrogen bonds, which the imidazolium head is able to establish [21–23], remain secondary under the reaction conditions of the EASA process. These results encourage further research with the purpose of achieving new ionic liquid-based functional hybrid materials, for example by applying the EASA method on mixtures of long and short chain imidazolium ionic liquids or on other yet unexplored ionic liquids structures.

CRediT authorship contribution statement

Szilvia Vavra: Conceptualization, Investigation, Writing - original draft, Writing - review & editing. **Neus Vilà:** Supervision. **Antiope Lotsari:** Formal analysis. **Alain Walcarius:** Supervision. **Anna Martinelli:** Funding acquisition, Supervision, Project administration.

Declaration of competing interest

The authors declare that they have no known competing financial interests or personal relationships that could have appeared to influence the work reported in this paper.

Acknowledgement

Funding from the Swedish Foundation for Strategic Research (SSF, grant no FFL-15 0092), from the Knut & Alice Wallenberg Foundation (Wallenberg Academy Fellow, grant no 2016-0220) and from the Swedish Research Council (grant no 2018–05207) is kindly acknowledged. All the authors thank Anne Wendel for performing the XPS experiments. This work was performed in part at the Chalmers Material Analysis Laboratory (CMAL). The technical help of Dr. Katarina Logg during the X-ray scattering measurements is greatly appreciated.

Appendix A. Supplementary data

Supplementary data to this article can be found online at https://doi.org/10.1016/j.micromeso.2020.110407.

References

[1] F. Yan, X. Lin, B. Su, Vertically ordered silica mesochannel films: electrochemistry and analytical applications, Analyst 141 (12) (2016) 3482–3495.
[2] K.C. Wu, X. Jiang, Y. Yamauchi, New trend on mesoporous films: precise controls of one-dimensional (1D) mesochannels toward innovative applications, J. Mater. Chem. 21 (25) (2011) 8934–8939.
[3] A. Walcarius, E. Sibottier, M. Etienne, J. Ghanbaja, Electrochemically assisted self-assembly of mesoporous silica thin films, Nat. Mater. 6 (8) (2007) 602–608.
[4] Y. Kanno, T. Suzuki, Y. Yamauchi, andK. Kuroda, Preparation of Au nanowire films by electrodeposition using mesoporous silica films as a template: vital effect of vertically oriented mesopores on a substrate, J. Phys. Chem. C 116 (46) (2012) 24672–24680.
[5] Z. Teng, G. Zheng, Y. Dou, W. Li, C.Y. Mou, X. Zhang, A.M. Asiri, D. Zhao, Highly ordered mesoporous silica films with perpendicular mesochannels by a simple stöber-solution growth approach, Angew. Chem. Int. Ed. 51 (9) (2012) 2173–2177.
[6] E.K. Richman, T. Brezesinski, S.H. Tolbert, Vertically oriented hexagonal mesoporous films formed through nanometre scale epitaxy, Nat. Mater. 7 (9) (2008) 712–717.
[7] M. Antonietti, D. Kuang, B. Smarsly, Y. Zhou, Ionic liquids for the convenient synthesis of functional nanoparticles and other inorganic nanostructures, Angew. Chem. Int. Ed. 43 (38) (2004) 4988–4992.
[8] A. Vioux, L. Viau, S. Volland, J. Le Bideau, Use of ionic liquids in sol-gel; ionogels and applications, Compt. Rendus Chem. 13 (1-2) (2010) 242–255.
[9] J. Dupont, From molten salts to ionic liquids: a "nano" journey, Acc. Chem. Res. 44 (11) (2011) 1223–1231.
[10] I. Abdurrokhman, K. Elamin, O. Danyliv, M. Hasani, J. Swenson, A. Martinelli, Protic ionic liquids based on the alkyl-imidazolium cation: effect of the alkyl chain length on structure and dynamics, J. Phys. Chem. B 9 (5) (2016) 1459–1464.
[11] R.E. Morris, Ionothermal synthesis - ionic liquids as functional solvents in the preparation of crystalline materials, Chem. Commun. (21) (2009) 2990–2998.
[12] R. Hayes, G.G. Warr, R. Atkin, Structure and nanostructure in ionic liquids, Chem. Rev. 115 (13) (2015) 6357–6426.
[13] H. Kaper, B. Smarsly, Templating and phase behaviour of the long chain ionic liquid C 16mimCl, Z. Phys. Chem. 220 (10-11) (2006) 1455–1471.
[14] Y. Zhou, J.H. Schattka, M. Antonietti, Room-temperature ionic liquids as template to monolithic mesoporous silica with wormlike pores via a sol-gel nanocasting technique, Nano Lett. 4 (3) (2004) 477–481.
[15] J. Łuczak, M. Paszkiewicz, A. Krukowska, A. Malankowska, A. Zaleska-Medynska, Ionic liquids for nano- and microstructures preparation. Part 1: properties and multifunctional role, Adv. Colloid Interface Sci. 230 (2016) 13–28.
[16] R. Dutta, S. Kundu, N. Sarkar, Ionic liquid-induced aggregate formation and their applications, Biophys. Rev. 10 (3) (2018) 861–871.
[17] T. Wang, H. Kaper, M. Antonietti, B. Smarsly, Templating behavior of a long-chain ionic liquid in the hydrothermal synthesis of mesoporous silica, Langmuir 23 (3) (2007) 1489–1495.
[18] H. Zhang, S. Liu, Preparation of ordered mesoporous silica materials templated by ionic liquids in alkaline condition, J. Porous Mater. 26 (1) (2019) 1–6.
[19] Y. Zhou, M. Antonietti, Preparation of highly ordered monolithic super-microporous lamellar silica with a room-temperature ionic liquid as template via the nanocasting technique, Adv. Mater. 15 (17) (2003) 1452–1455.
[20] Y. Zhou, M. Antonietti, A series of highly ordered, Super Microporous, lamellar silicas prepared by nanocasting with ionic liquids, Chem. Mater. 16 (3) (2004) 544–550.
[21] J. Thar, M. Brehmy, A.P. Seitsonen, B. Kirchner, Unexpected hydrogen bond dynamics in imidazolium-based ionic liquids, J. Phys. Chem. B 113 (46) (2009) 15129–15132.
[22] M. Kohagen, M. Brehm, Y. Lingscheid, R. Giernoth, J. Sangoro, F. Kremer, S. Naumov, C. Iacob, J. Kärger, R. Valiullin, B. Kirchner, How hydrogen bonds influence the mobility of imidazolium based ionic liquids. A combined theoretical

and experimental study of 1-n-butyl-3- methylimidazolium bromide, J. Phys. Chem. B 115 (51) (2011) 15280–15288.
[23] H. Watanabe, H. Doi, S. Saito, M. Matsugami, K. Fujii, R. Kanzaki, Y. Kameda, Y. Umebayashi, Hydrogen bond in imidazolium based protic and aprotic ionic liquids, J. Mol. Liq. 217 (2016) 35–42.
[24] F. Tang, T. Ohto, T. Hasegawa, M. Bonn, Y. Nagata, Π+Π+ stacking of imidazolium cations enhances molecular layering of room temperature ionic liquids at their interfaces, Phys. Chem. Chem. Phys. 19 (4) (2017) 2850–2856.
[25] Y.L. Wang, A. Laaksonen, M.D. Fayer, Hydrogen bonding versus π-π stacking interactions in imidazolium-oxalatoborate ionic liquid, J. Phys. Chem. B 121 (29) (2017) 7173–7179.
[26] M. Zhao, Y. Gao, L. Zheng, Liquid crystalline phases of the amphiphilic ionic liquid n -hexadecyl- n -methylpyrrolidinium bromide formed in the ionic liquid ethylammonium nitrate and in water, J. Phys. Chem. B 114 (35) (2010) 11382–11389.
[27] S. Hudson, D.A. Tanner, W. Redington, E. Magner, K. Hodnett, S. Nakahara, Quantitative TEM analysis of a hexagonal mesoporous silicate structure, Phys. Chem. Chem. Phys. 8 (29) (2006) 3467–3474.
[28] A. Martinelli, M. Maréchal, Å. Östlund, J. Cambedouzou, Insights into the interplay between molecular structure and diffusional motion in 1-alkyl-3-methylimidazolium ionic liquids: a combined PFG NMR and X-ray scattering study, Phys. Chem. Chem. Phys. 15 (15) (2013) 5510–5517.
[29] A. Goux, M. Etienne, E. Aubert, C. Lecomte, J. Ghanbaja, A. Walcarius, Oriented mesoporous silica films obtained by electro assisted self-assembly (EASA), Chem. Mater. 21 (4) (2009) 731–741.
[30] M.P. Tate, H.W. Hillhouse, General method for simulation of 2D GISAXS intensities for any nanostructured film using discrete fourier transforms, J. Phys. Chem. C 111 (21) (2007) 7645–7654.
[31] J. Choi, I. Gunkel, Y. Li, Z. Sun, F. Liu, H. Kim, K.R. Carter, T.P. Russell, Macroscopically ordered hexagonal arrays by directed self assembly of block copolymers with minimal topographic patterns, Nanoscale 9 (39) (2017) 14888–14896.
[32] Y. Guillemin, M. Etienne, E. Aubert, A. Walcarius, Electrogeneration of highly methylated mesoporous silica thin films with vertically-aligned mesochannels and electrochemical monitoring of mass transport issues, J. Mater. Chem. 20 (32) (2010) 6799–6807.
[33] S. Ahoulou, N. Vilà, S. Pillet, D. Schaniel, A. Walcarius, Coordination polymers as template for mesoporous silica films: a novel Composite Material Fe(Htrz)3@SiO2withRemarkable electrochemical properties, Chem. Mater. 31 (15) (2019) 5796–5807.
[34] P. Innocenzi, Infrared spectroscopy of sol – gel derived silica based films : a spectra-microstructure overview, J. Non-Cryst. Solids 316 (2003) 309–319.
[35] Y. Guillemin, J. Ghanbaja, E. Aubert, M. Etienne, A. Walcarius, Electro-assisted self-assembly of cetyltrimethylammonium-templated silica films in aqueous media: critical effect of counteranions on the morphology and mesostructure type, Chem. Mater. 26 (5) (2014) 1848–1858.
[36] A. Goux, J. Ghanbaja, A. Walcarius, Prussian Blue electrodeposition within an oriented mesoporous silica film: preliminary observations, J. Mater. Sci. 44 (24) (2009) 6601–6607.
[37] M. Etienne, Y. Guillemin, D. Grosso, A. Walcarius, Electrochemical approaches for the fabrication and/or characterization of pure and hybrid templated mesoporous oxide thin films: a review, Anal. Bioanal. Chem. 405 (5) (2013) 1497–1512.
[38] T. Nasir, G. Herzog, M. Hébrant, C. Despas, L. Liu, A. Walcarius, Mesoporous silica thin films for improved electrochemical detection of paraquat, ACS Sens. 3 (2) (2018) 484–493.
[39] C. Karman, N. Vilà, A. Walcarius, Amplified charge transfer for anionic redox probes through oriented mesoporous silica thin films, ChemElectroChem 3 (12) (2016) 2130–2137.
[40] N. Vilà, P. de Oliveira, A. Walcarius, I.M. Mbomekallé, pH modulated ion transport and amplified redox response of Keggin type polyoxometalates through vertically-oriented mesoporous silica nanochannels, Electrochim. Acta 309 (2019) 209–218.
[41] N. Vilà, E. André, R. Ciganda, J. Ruiz, D. Astruc, A. Walcarius, Molecular sieving with vertically aligned mesoporous silica films and electronic wiring through isolating nanochannels, Chem. Mater. 28 (8) (2016) 2511–2514.
[42] X. Lin, Q. Yang, L. Ding, B. Su, Ultrathin silica membranes with highly ordered and perpendicular nanochannels for precise and fast molecular separation, ACS Nano 9 (11) (2015) 11266–11277.